Dinuclear Copper(II) Complexes Incorporating a New Septadentate Polyimidazole Ligand

Hanlin Nie,[†] Sheila M. J. Aubin,[‡] Mark S. Mashuta,[†] Richard A. Porter,[†] John F. Richardson,[†] David N. Hendrickson,*[,‡] and Robert M. Buchanan*[,†]

Departments of Chemistry, University of Louisville, Louisville, Kentucky 40292, and University of California, San Diego, La Jolla, California 92093-0358

Received September 15, 1995[⊗]

The dinuclear copper(II) complexes $[Cu_2(tmihpn)(prz)](ClO_4)_2 \cdot 2CH_3CN$ (**6**) and $[Cu_2(tmihpn)(O_2CCH_3)](ClO_4)_2 \cdot CH_3CN$ (**7**) were prepared, where tmihpn is the deprotonated form of *N*,*N*,*N*′,*N*′-tetrakis[(1-methylimidazol-2-yl)-methyl]-1,3-diaminopropan-2-ol and prz is the pyrazolate anion. The crystal structures of **6** and **7** were determined and revealed that both complexes contain bridging alkoxide ligands as well as bridging pyrazolate and acetate ions, respectively. Crystal data: compound **6**, triclinic, $P\bar{1}$, $a = 18.089(2)$ Å, $b = 22.948(3)$ Å, $c = 9.597(2)$ Å, $\alpha = 93.37(2)°$, $\beta = 94.49(2)°$, $\gamma = 81.69(2)°$, $V = 3925.1$ Å^3, $Z = 4$; compound **7**, triclinic, $P\bar{1}$, $a = 12.417(2)$ Å, $b = 15.012(3)$ Å, $c = 10.699(2)$ Å, $\alpha = 104.76(2)°$, $\beta = 102.63(2)°$, $\gamma = 99.44(2)°$, $V = 1830.1$ Å^3, $Z = 2$. In compound **6**, the coordination geometry around both copper centers resembles a distorted square pyramid, while the stereochemistry around the copper centers in **7** is best described as trigonal bipyramidal. Both complexes display well-resolved isotropically shifted ^{1}H NMR spectra. Selective substitution studies and integration data have been used to definitively assign several signals to specific ligand protons. Results from the solution ^{1}H NMR studies suggest that the basal and apical imidazole groups do not exchange rapidly on the NMR time scale and the solid state structures of the complexes are retained in solution. In addition, the magnetochemical characteristics of **6** and **7** were determined and provide evidence for "magnetic orbital switching". Antiferromagnetic coupling in **6** ($J = -130$ cm^{-1}) is strong, while the copper centers in compound **7** are ferromagnetically coupled ($J = +16.4$ cm^{-1}). Differences in the magnetic behavior of the two copper centers have been rationalized using the "ligand orbital complementary" concept. The ground state magnetic orbitals involved in spin coupling in **6** ($d_{x^2-y^2}$) are different from those in **7** (d_{z^2}).

Introduction

Magnetism has played an important role in the development of our understanding of the structural and electronic factors that govern spin exchange phenomena in inorganic and bioinorganic systems.[1] The detection of magnetic exchange coupling between paramagnetic metal centers has been particularly useful in deducing the structures of polynuclear metal compounds and the active sites of much larger metallobiomolecules.[2] For instance, dinuclear copper proteins such as hemocyanin[3−6] and tyrosinase[6−9] are thought to have similar active site structures, yet they perform different chemical functions. The structure[10,11] of oxyhemocyanin (oxyHc) from *Limulus* has revealed the presence of a μ-η^2:η^2 peroxo-bridged unit that results in a strong magnetic exchange coupling between Cu(II) ions and the EPR silence associated with type III copper proteins.[12,13] Strong

* Authors to whom correspondence should be addressed.
[†] University of Louisville.
[‡] University of California.
[⊗] Abstract published in *Advance ACS Abstracts,* May 1, 1996.

(1) (a) Reed, C. A.; Orosz, R. D. In *Research Frontiers in Magnetochemistry*; O'Connor, C. J., Ed.; World Scientific Publishing Co.: New York, 1993. (b) Hendrickson, D. N. In *Magneto-Structural Correlations in Exchange Coupled Systems*; Willet, R., Gatteschi, D., Kahn, O., Eds.; Reidel: Dordrecht, Holland, 1984. (c) Solomon, E. I.; Wilcox, D. E. In *Magneto-Structural Correlations in Exchange Coupled Systems*; Willet, R., Gatteschi, D., Kahn, O., Eds.; Reidel: Dordrecht, Holland, 1985. (d) Coffman, R. E.; Buettner, G. R. *J. Phys. Chem.* **1979**, *83*, 2387. (e) Gerloch, M.; Harding, J. H. *Proc. R. Soc. London* 1978, *A360*, 211. (f) Duggan, D. M.; Hendrickson, D. N. *Inorg. Chem.* **1973**, *12*, 2422. (g) Felthouse, T. R.; Laskowski, E. J.; Hendrickson, D. N. *Inorg. Chem.* **1977**, *16*, 1077. (h) Julve, M.; Verdaugher, M.; Kahn, O.; Gleizes, A.; Philoche-LeVisalles, M. *Inorg. Chem.* **1983**, *22*, 368. (i) Kahn, O.; Briat, B. *J. Chem. Soc., Faraday Trans.* **1976**, 268. (j) DeLoth, P.; Cassoux, P.; Daudey, J. P.; Malrieu, J. P. *J. Am. Chem. Soc.* **1981**, *103*, 4007. (k) *Theory and Applications of Molecular Paramagnetism*; Boudreaux, E. A., Mulay, L. N., Eds.; J. Wiley & Sons: New York 1976.
(2) Bencini, A.; Gatteschi, D. *Inorg. Chim. Acta* **1978**, *31*, 11.
(3) Solomon, E. I.; Penfield, K. W.; Wilcox, D. E. *Struct. Bonding (Berlin)* **1983**, *53* , 1−57.
(4) Bannister, J. V. *Structure and Function of Hemocyanin*; Springer-Verlag: Berlin, Heidelberg, New York, 1977.
(5) Solomon, E. I. In *ACS Symposium Series 372*; Que, L., Jr., Ed.; American Chemical Society: Washington, DC, 1988; pp 116−150.
(6) (a) Karlin, K. D.; Gultneh, Y. *J. Chem. Educ.* **1985**, *62*, 983−990. (b) Karlin, K. D.; Gultneh, Y. *Prog. Inorg. Chem.* **1987**, *35*, 219−327.
(7) (a) Jolley, R. L. J.; Evans, L. H.; Makino, N.; Mason, H. S. *J. Biol. Chem.* **1974**, *249*, 335−345. (b) Mason, H. S.; Fowlks, W. B.; Peterson, E. W. *J. Am. Chem. Soc.* **1955**, *77*, 2914−2915.
(8) (a) Eickman, N. C.; Solomon, E. I.; Larrabee, J. A.; Spiro, T. G.; Lerch, K. *J. Am. Chem. Soc.* **1978**, *100* , 6529−6531. (b) Himmelwright, R. S.; Eickman, N. C.; LuBien, C. D.; Lerch, K.; Solomon, E. I. *J. Am. Chem. Soc.* **1980**, *102*, 7339−7344. (c) Lerch, K. *Met. Ions Biol. Syst.* **1981**, *13* , 143−186. (d) Solomon, E. I. In *Copper Coordination Chemistry: Biochemical & Inorganic Perspectives*; Karlin, K. D., Zubieta, J., Eds.; Adenine: Guilderland, NY, 1983; pp 1−22. (e) Wilcox, D. E.; Porras, A. G.; Hwang, Y. T.; Lerch, K.; Winkler, M. E.; Solomon, E. I. *J. Am. Chem. Soc.* **1985**, *107* , 4015−4027.
(9) Robb, D. A. In *Copper Proteins and Copper Enzymes*; Lontie, R., Ed.; CRC: Boca Raton, FL, 1984; Vol. 2; pp 207−241.
(10) Magnus, K.; Ton-That, H. J. *J. Inorg. Biochem.* **1992**, *47* , 20.
(11) Kitajima, N.; Koda, T.; Hashimoto, S.; Kitagawa, T.; Moro-oka, Y. *J. Chem. Soc., Chem. Commun* **1988**, 151−152.
(12) Moss, T. H.; Gould, D. C.; Ehrenberg, A.; Loehr, J. S.; Mason, H. S. *Biochemistry* **1973**, *12*, 2444−2449.
(13) (a) Solomon, E. I.; Dooley, D. M.; Wang, R. H.; Gray, H. B.; Cerdonio, M.; Mogno, F.; Romani, G. L. *J. Am. Chem. Soc.* **1976**, *98*, 1029−1031. (b) Dooley, D. M.; Scott, R. A.; Ellingham, J.; Solomon, E. I.; Gray, H. B. *Proc. Natl. Acad. Sci. U.S.A.* **1978**, *75*, 3019−3022.
(14) (a) Kitajima, N.; Fujisawa, K.; Fujimoto, C.; Moro-oka, Y.; Hashimoto, S.; Kitagawa, T.; Toriumi, K. Tatsumi, K.; Nakamura, A. *J. Am. Chem. Soc.* **1992**, *114* , 1277−1291. (b) Kitajima, N.; Fujisawa, K.; Moro-oka, Y.; Toriumi, K. *J. Am. Chem. Soc.* **1989**, *111* , 8975−8976.
(15) Ross, P. K.; Solomon, E. I. *J. Am. Chem. Soc.* **1991**, *113*, 3246−3259.

S0020-1669(95)01198-0 CCC: $12.00

antiferromagnetic exchange coupling also is observed for a model complex, $[Cu(HB(3,5\text{-}iPr_2pz)_3)]_2(O_2)$,[14] which has a similar $\mu\text{-}\eta^2\text{:}\eta^2$ peroxo-bridged structure.

Extended Hückel[14a] and SCF−Xα−SW[15] calculations on oxyHc and $[Cu(HB(3,5\text{-}iPr_2pz)_3)]_2(O_2)$ are in good agreement with the results of Hoffmann *et al.*[16] and others[2,17] that rationalize the strength of the exchange interaction involving different bridging ligands in terms of differences in the symmetries of magnetic orbitals involved in the superexchange process. Therefore the diamagnetism of oxyHc and $[Cu(HB(3,5\text{-}iPr_2pz)_3)]_2(O_2)$ results from the large energy gap between the HOMO/LUMO levels, and the dominant magnetic exchange pathway involves the antisymmetric combination of d_a associated with the $d_{x^2-y^2}$ orbital of the metal and the π^* level of the bridging peroxo ligand. This combination is destabilized relative to the symmetric combination (d_s) which results in an increase in the antiferromagnetic exchange coupling.

Magnetic properties of related doubly bridged Cu^{II}_2 complexes also have been the subject of intense investigation.[3,18−20] For instance, the magnetic exchange characteristics of the azido-bridged complex $[Cu_2(L\text{-}Et)N_3]^{2+}$ [21] have been studied extensively as a model of azidomethemocyanin, met(N_3)Hc.[19,20] $[Cu_2(L\text{-}Et)N_3]^{2+}$ and met(N_3)Hc are both diamagnetic resulting from strong antiferromagnetic exchange coupling, and the strength of the exchange interaction has been adequately explained in terms of bridging ligand orbital complementarity. As with oxyHc and $[Cu(HB(3,5\text{-}iPr_2pz)_3)]_2(O_2)$, the two bridging ligands in $[Cu_2(L\text{-}Et)N_3]^{2+}$ act in concert to destabilize the antisymmetric combination (d_a) relative to the symmetric combination (d_s) which leads to strong magnetic exchange coupling.

Herein we describe our latest efforts to correlate the magnetic and structural properties of two new dinuclear Cu^{II} complexes resulting from the polyimidazole ligand *N,N,N′,N′*-tetrakis-[(1-methylimidazol-2-yl)methyl]-1,3-diaminopropan-2-ol (Htmihpn). Details of the synthesis, crystal structures, and ^{1}H NMR spectra of the acetate- and pyrazolate-bridged Cu^{II}_2 complexes of tmihpn as well as magnetostructural correlations of both complexes that provide direct evidence of "magnetic orbital switching" are presented.

Experimental Section

All reagents and solvents used in this study were commercially available and were used as received. Solvents were dried by conventional procedures prior to use. N,N′-Bis[(1-methylimidazol-2-yl)-methylene]-1,3-diaminopropan-2-ol (**1**)[22] and 2-(chloromethyl)-1-methylimidazole hydrochloride (**2**)[23] were prepared by following previously reported procedures. All samples were thoroughly dried prior to elemental analyses, which were performed by Midwest Analytical, Inc., Indianapolis, IN.

Ligand Synthesis. (a) *N,N′*-Bis[(1-methylimidazol-2-yl)methyl]-1,3-diaminopropan-2-ol (3). To a solution containing 3.21 g (11.7 mmol) of compound **1** and 120 mL of dry methanol was added 1.33 g (35.1 mmol) of $NaBH_4$. The mixture was stirred for 2 h, and the reaction was then quenched by addition of 1 mL of 5 N HCl. The precipitate was filtered off, and the resulting filtrate was taken to dryness. The crude product was dissolved in 5 mL of water and extracted with three 30 mL portions of $CHCl_3$. The combined extracts were dried with $MgSO_4$. The $CHCl_3$ was then removed under reduced pressure to give 3.05 g (yield 94%) of compound **3**. The hydrochloride salt of compound **3** was prepared by passing HCl gas through a methanol solution of compound **3**, affording a white precipitate. Anal. Calcd for $C_{13}H_{22}N_6O\cdot4HCl$: C, 36.81; H, 6.17; N, 19.81. Found: C, 36.56; H, 5.90; N, 19.47. ^{1}H NMR (DMSO, δ): 2.48 (m, 4 H), 3.59 (s, 6 H), 3.63 (s, 1 H), 3.69 (s, 4 H), 6.72 (s, 2 H), 7.01 (s, 2 H), 8.32 (s, 2 H). ^{13}C NMR (DMSO, δ): 32.13 (ImN−*C*H$_3$), 45.09 (1,3-*C*H$_2$), 53.44 (Im−*C*H$_2$−N), 68.52 (CH$_2$−*C*H(OH)−CH$_2$), 121.35 (Im*C*−H), 125.84 (Im*C*−H), 146.36 (Im*C*−CH$_2$).

(b) *N,N,N′,N′*-Tetrakis[(1-methylimidazol-2-yl)methyl]-1,3-diaminopropan-2-ol (5). To a solution containing 3.04 g (18.2 mmol) of compound **2** and 30 mL of dry acetonitrile was added 1.84 g (18.2 mmol) of triethylamine under N_2. The reaction mixture was allowed to stir at 0 °C for 1 h and then filtered. The solution containing the free base of 2-(chloromethyl)-1-methylimidazole (**4**) was added immediately to an acetonitrile solution containing 2.53 g (9.10 mmol) of compound **3** and 1.93 g (19.1 mmol, 5% excess with respect to the stoichiometric amount) of triethylamine. The reaction mixture was allowed to stir at room temperature under a N_2 atmosphere for 48 h. The resulting slurry was evaporated *in vacuo* to 10 mL. The resulting precipitate was filtered off and the filtrate was taken to dryness *in vacuo*. The crude product, dissolved in 10 mL of CH_2Cl_2, was loaded onto a neutral alumina column (35 × 2 cm) and eluted with 200 mL of a CH_2Cl_2−MeOH (10:1) mixture. The solvents were removed under reduced pressure, affording 3.55 g (overall yield 69%) of compound **5**. Anal. Calcd for $C_{23}H_{36}N_{10}O_2$: C, 57.00; H, 7.48; N, 28.90. Found: C, 56.96; H, 7.42; N, 28.69. ^{1}H NMR ($CDCl_3$, δ): 2.49 (m, 4 H), 3.46 (s, 12 H), 3.72 (d, 9 H), 6.75 (s, 4 H), 6.86 (s, 4 H). ^{13}C NMR ($CDCl_3$, δ): 32.54 (ImN−*C*H$_3$), 51.06 (1,3-*C*H$_2$), 59.47 (Im−*C*H$_2$−N), 68.15 (CH$_2$−*C*H(OH)−CH$_2$), 121.36 (Im*C*−H), 126.90 (Im*C*−H), 145.73 (Im*C*−CH$_2$).

Synthesis of Metal Complexes. (a) $[Cu_2(tmihpn)(prz)](ClO_4)_2\cdot 2CH_3CN$ (6). To an ethanol solution (20 mL) containing 0.52 g (1.1 mmol) of compound **5**, 0.33 g (3.3 mmol) of triethylamine, and 0.08 g (1.1 mmol) of pyrazole was added slowly 0.82 g (2.2 mmol) of $Cu(ClO_4)_2\cdot6H_2O$ dissolved in 10 mL of ethanol. The reaction mixture was stirred overnight, and the greenish-blue precipitate was isolated by filtration. The complex was recrystallized from acetonitrile by slow evaporation, yielding 0.74 g (72%) of X-ray grade crystals. Anal. Calcd for $Cu_2C_{26}H_{36}N_{12}Cl_2O_9\cdot{}^1/_2H_2O$ (the dried sample is slightly hygroscopic): C, 35.99; H, 4.33; N, 18.90. Found: C, 36.16; H, 4.33; N, 18.90.

(b) $[Cu_2(tmihpn)(O_2CCH_3)](ClO_4)_2\cdot CH_3CN$ (7). Compound **7** was prepared following the same procedure described above for compound **6** with two exceptions: sodium acetate was substituted for pyrazole, and 1 equiv of triethylamine was added to the reaction mixture instead of 3 equiv of base. The resulting greenish-blue precipitate was recrystallized from acetonitrile by slow evaporation, affording crystals of **7** (yield 65%) that were suitable for X-ray crystallographic studies. Anal. Calcd for $Cu_2C_{25}H_{36}N_{10}Cl_2O_{11}$: C, 35.30; H, 4.27; N, 16.47. Found: C, 35.32; H, 4.30; N, 16.50.

$[Cu_2(htmihpn)(O_2CCD_3)](ClO_4)$ was prepared by following the same procedure as described above substituting NaO_2CCD_3 for NaO_2CCH_3 and used in ^{1}H NMR studies (vide infra).

(16) Hay, P. J.; Thibeault, J. C.; Hoffmann, R. *J. Am. Chem. Soc.* **1975**, *97*, 4884−4899.
(17) (a) Kahn, O. *Inorg. Chim. Acta* **1982**, *62*, 3. (b) Astheimer, H.; Haase, W. *J. Chem. Phys.* **1986**, *85*, 1427.
(18) (a) Solomon, E. I.; Allendorf, M. D.; Kau, L.-S.; Pate, J. E.; Spira-Solomon, D.; Wilcox, D. E.; Porras, A. G. *Life Chem. Rep.* **1987**, *5*, 37−89. (b) Himmelwright, R. S.; Eickman, N. C.; Solomon, E. I. *Biochem. Biophys. Res. Commun.* **1979**, *86*, 628. (c) Himmelwright, R. S.; Eickman, N. C.; Solomon, E. I. *Biochem. Biophys. Res. Commun.* **1978**, *84*, 300. (d) Himmelwright, R. S.; Eickman, N. C.; Solomon, E. I. *Biochem. Biophys. Res. Commun.* **1978**, *81*, 237. (e) Himmelwright, R. S.; Eickman, N. C.; Solomon, E. I. *Biochem. Biophys. Res. Commun.* **1978**, *81*, 233.
(19) Pate, J. E.; Ross, P. K.; Thamann,T. J.; Reed, C. A.; Karlin, K. D.; Sorrel, T. N.; Solomon, E. I. *J. Am. Chem. Soc.* **1989**, *111*, 5198−5209.
(20) (a) Woolelery, G. L.; Powers, L.; Winkler, M.; Solomon, E. I.; Spiro, T. G. *J. Am. Chem. Soc.* **1984**, *106*, 86−92. (b) Pate, J. E.; Thamann,T. J.; Solomon, E. I. *Spectrochim. Acta* **1986**, *42A*, 313. (c) Himmelwright, R. S.; Eickman, N. C.; LuBien, C. D.; Solomon, E. I. *J. Am. Chem. Soc.* **1980**, *102*, 5378−5388.
(21) (a) McKee, V.; Zvagulis, M.; Dagdigian, J. C.; Patch, M. G.; Reed, C. A. *J. Am. Chem. Soc.* **1984**, *106*, 4765−4772. (b) McKee, V.; Dagdigian, J. C.; Bau, R.; Reed, C. A. *J. Am. Chem. Soc.* **1981**, *103*, 7000−7001.
(22) Doman, T. N.; Richardson, J. F.; Arar, L.; Buchanan, R. M. *Inorg. Chim. Acta* **1989**, *159*, 219−224.
(23) Vaira, M. D.; Mani, F.; Stoppioni, P. *J. Chem. Soc., Chem. Commun.* **1989**, 126−127.

Table 1. Crystallographic Data for Compounds **6** and **7**

	6	**7**
formula	$Cu_2C_{30}H_{42}N_{14}Cl_2O_9$	$Cu_2C_{27}H_{39}N_{11}Cl_2O_{11}$
fw	940.74	891.66
a, Å	18.089(2)	12.417(2)
b, Å	22.948(3)	15.012(3)
c, Å	9.597(2)	10.699(2)
α, deg	93.37(2)	104.76(2)
β, deg	94.49(2)	102.63(2)
γ, deg	81.69(2)	99.44(2)
V, Å^3	3925.1	1830.1
Z	4	2
space group	$P\bar{1}$ (No. 2)	$P\bar{1}$ (No. 2)
ρ_{calc}, g/cm^3	1.59	1.61
ρ_{obs}, g/cm^3	1.58	1.61
abs coeff, cm^{-1}	12.9	13.8
radiation (*λ*, Å)	Mo Kα (0.710 73)	Mo Kα(0.7107 3)
temp, K	195(5)	195(5)
R^a	0.079	0.072
$R_w{}^b$	0.104	0.078
GOF	1.00	1.56

^{a} $R = \sum(||F_o| - |F_c||)/\sum|F_o|$. ^{b} $R_w = [\sum w(|F_o| - |F_c|)^2/\sum w|F_o|^2]^{1/2}$; $w = [\sigma(F)^2 + (0.01F)^2 + 1.5]^{-1}$.

Caution! Perchlorate salts of metal complexes are potentially explosive and should be handled in small quantities with care.

Physical Measurements. UV-visible spectra were recorded using a Hewlett Packard HP8452A diode-array spectrophotometer. ^{1}H and ^{13}C NMR spectra were obtained using either a Varian XL-300 or a Bruker AMX-500 spectrometer. The variable-temperature solid-state magnetic susceptibility data were collected on a Quantum Design MPMS5 SQUID susceptometer equipped with a 55 kG magnet and operating in the range 1.8−400 K. Diamagnetic corrections were estimated using Pascal's constants and were subtracted from the experimental molar susceptibility to obtain the paramagnetic molar susceptibility.[1k]

X-ray Data Collection and Reduction. Blue crystals of $[Cu_2(htmihpn)(prz)](ClO_4)_2\cdot 2CH_3CN$ **(6)** and $[Cu_2(htmihpn)(O_2CCH_3)](ClO_4)_2\cdot CH_3CN$ (**7**) were mounted on glass fibers and coated with epoxy prior to data collection. Crystals were aligned, and X-ray intensity data were collected using an Enraf-Nonius CAD-4 diffractometer equipped with a graphite monochromator (Mo Kα radiation, $\lambda = 0.710\,73$ Å). Crystallographic data for both complexes are summarized in Table 1. Lattice parameters for both complexes were obtained from least-squares analyses of 25 centered reflections with $20° \le 2\theta \le 32°$ and $18° \le 2\theta \le 22°$ for **6** and **7**, respectively. Data were collected using the $\omega-2\theta$ scan technique to maximum 2θ values of 50° with 13 787 and 6424 independent reflections for compounds **6** and **7**, respectively; of these, 11 671 and 5615 were considered observed with $I > 3\sigma(I)$. The intensities of three standard reflections were monitored every 60 min during data collection on both complexes. Neither compound showed significant decay during data collection. Intensity data were corrected for Lorentz and polarization effects. An empirical absorption correction based on DIFABS[24] was applied to the data for compound **6**, which resulted in transmission factors ranging from 0.817 to 0.992.

Structure Solution and Refinement. The structures were solved using direct methods (MULTAN)[25] and refined by full-matrix least-squares techniques minimizing the function $\sum w(|F_o| - |F_c|)^2$. All non-hydrogen atoms, with the exception of the O atoms of the disordered ClO_4^- and some solvent molecules, were refined anisotropically. Hydrogen atom positions for both complexes were calculated and included as fixed contributions ($B_{iso} = 1.2B_{iso}$ of attached atom) during the final cycles of least-squares refinement. The asymmetric unit of compound **6** consists of two independent cations and four disordered ClO_4^- anions as well as four CH_3CN molecules. A total of 986 variables were used in the final cycles of least-squares refinement of **6**. The asymmetric unit of compound **7** consists of a single cation, two ClO_4^- anions (one of which is disordered), and one CH_3CN molecule. A total of 482 variables were used in the final cycle of least-squares refinement of **7**. Tables 2 and 3 contain all the non-hydrogen atomic positional parameters for compounds **6** and **7**, respectively. Final difference Fourier maps showed no significant residual electron density.

Results and Discussion

Synthesis. The ligand Htmihpn (**5**) was synthesized as shown in Scheme 1. The secondary amine (**3**) is readily prepared by reduction of the Schiff base (**1**) with $NaBH_4$. The free base of 2-(chloromethyl)-1-methylimidazole (**4**) is prepared by reacting the hydrochloride salt of **2** with a stoichiometric quantity of triethylamine in dry acetonitrile at 0 °C. Compound **5,** on the other hand, may be prepared by stirring a solution containing stoichiometric quantities of **3** and **4** and a slight excess (5%) of triethylamine under nitrogen for 48 h. The crude product of **5** was purified either by extraction from aqueous solution, by precipitation as a hydrochloride salt, or by chromatography. The last method appears to be the most efficient way to purify compound **5**. In a general procedure, the crude product of compound **5**, dissolved in CH_2Cl_2, is loaded onto a neutral alumina column and eluted with $CH_2Cl_2-CH_3OH$ (10:1). The structure and purity of compound **5** have been confirmed by TLC and ^{1}H and ^{13}C NMR as well as by elemental analysis.

The copper(II) complexes of the ligand, $[Cu_2(htmihpn)X](ClO_4)_2$ (where X = acetate and pyrazolate), were prepared by mixing stoichiometric quantities of Htmihpn, $Cu(ClO_4)_2\cdot 6H_2O$, and the appropriate bridging ligand in the presence of triethylamine in ethanol. The reaction mixtures were allowed to stir overnight. The resulting blue precipitates were collected by filtration and recrystallized from acetonitrile by slow evaporation.

Description of Crystal Structures. (a) $[Cu_2(tmihpn)(prz)](ClO_4)_2\cdot 2CH_3CN$ (6). An ORTEP view of the cation of **6A** is shown in Figure 1. Selected bond distances and angles are given in Tables 4 and 5. The complex crystallizes with two independent dinuclear cations per asymmetric unit. Both cations have similar molecular structures and bonding parameters; the coordination geometry around each copper center is best described as distorted square pyramidal. The Cu−Cu separations in **6A** and **6B** are 3.320(1) and 3.3462(9) Å, respectively, and are comparable to the separation of 3.325(2) Å reported for the $[Cu_2(L\text{-}Et)(NO_2)]^{2+}$ cation[26] where L-Et is the binucleating ligand *N*,*N*,*N*′,*N*′-tetrakis[2-(1-ethylbenzimidazolyl)]-2-hydroxy-1,3-diaminopropane. For compound **6A**, Cu(1)−O(1) = 1.955(4) and Cu(2)−O(1) = 1.953(4) Å, while in compound **6B**, the Cu(1′)−O(1′) and Cu(2′)−O(1′) distances are 1.936(5) and 1.950(4) Å, respectively. The Cu−N(amine) bond lengths are 2.100(5) (Cu(1)−N(1)) and 2.101(6) Å (Cu(2)−N(6)) for **6A** and 2.129(6) (Cu(1′)−N(1′)) and 2.082-(5) Å (Cu(2′)−N(6′)) for **6B**, respectively. In both cations, the imidazole nitrogen atoms are bonded in both the apical (N(2) and N(7)) and equatorial (N(4) and N(9)) coordination sites. As expected, the apical bonds are longer than the equatorial bonds. The Cu−N(imidazole) bond lengths are 2.176(5) (Cu-(1)−N(2)), 2.007(5) (Cu(1)−N(4)), 2.197(6) (Cu(2)−N(7)), and 2.005(5) Å (Cu(2)−N(9)) for **6A** and 2.207(6) (Cu(1′)−N(2′)), 1.978(6) (Cu(1′)−N(4′)), 2.139(6) (Cu(2′)−N(7′)), and 2.042-(5) Å (Cu(2′)−N(9′)) for **6B**, respectively. The bridging pyrazolate ligands of both cations lie in the equatorial plane of

(24) Walker, N.; Stuart, D. *Acta Crystallogr.* **1983**, *A39*, 158−166.
(25) All crystallographic programs were part of the program package MolEN: *Mo1EN: An International Structure Solution Procedure*, Enraf-Nonius: Delft, The Netherlands, 1990. MULTAN: Main, P.; Fiske, S. J.; Hull, S. E.; Lessinger, L.; Germain, G.; Declercq, J. P.; Woolfson, M. M. (1980). *MULTAN 80: A System of Computer Programs for the Automatic Solution of Crystal Structures from X-ray Diffraction Data*; University of York: York, England, 1980.
(26) McKee, V.; Zvagulis, M.; Reed, C. A. *Inorg. Chem.* **1989**, *24*, 2914−2919.

Table 2. Positional Parameters with Estimated Standard Deviations and Thermal Parameters for Compound **6**

atom	*x*	*y*	*z*	*B*,[a] Å^2	atom	*x*	*y*	*z*	*B*,[a] Å^2
Cu(1)	0.63526(4)	0.10281(3)	0.64165(7)	1.71(1)	C(6′)	0.2010(5)	0.6558(4)	1.054(1)	4.1(2)
Cu(2)	0.79185(4)	0.01787(3)	0.55900(7)	2.01(1)	C(7′)	0.1729(5)	0.6986(3)	0.815(1)	4.3(2)
O(1)	0.7020(2)	0.0284(2)	0.6632(4)	1.87(7)	C(8′)	0.0803(4)	0.4979(3)	0.7086(8)	3.0(1)
N(1)	0.6068(3)	0.0847(2)	0.8410(5)	1.63(8)	C(9′)	0.0630(3)	0.4601(3)	0.8164(7)	2.3(1)
N(2)	0.5232(3)	0.0802(2)	0.5917(5)	2.00(9)	C(10′)	0.0724(4)	0.4122(3)	1.0078(7)	3.0(1)
N(3)	0.4337(3)	0.0364(2)	0.6717(5)	2.11(9)	C(11′)	0.0041(4)	0.4081(4)	0.9421(9)	3.5(1)
N(4)	0.6203(3)	0.1868(2)	0.7169(5)	2.13(9)	C(12′)	−0.0663(4)	0.4447(4)	0.7188(9)	3.9(2)
N(5)	0.6029(3)	0.2465(2)	0.9002(5)	2.09(9)	C(13′)	0.3369(3)	0.4240(3)	0.5820(6)	1.8(1)
N(6)	0.8305(3)	−0.0419(2)	0.7150(5)	2.05(9)	C(14′)	0.4589(3)	0.4557(3)	0.6708(6)	2.1(1)
N(7)	0.7941(3)	−0.0662(3)	0.4363(6)	2.8(1)	C(15′)	0.5070(3)	0.4460(3)	0.8019(6)	2.0(1)
N(8)	0.7768(4)	−0.1601(3)	0.4590(7)	3.2(1)	C(16′)	0.5419(3)	0.4223(3)	1.0159(6)	2.0(1)
N(9)	0.8976(3)	0.0356(2)	0.5753(6)	2.13(9)	C(17′)	0.5953(4)	0.4525(3)	0.9700(7)	2.5(1)
N(10)	1.0024(3)	0.0277(3)	0.7101(6)	2.6(1)	C(18′)	0.6107(4)	0.5007(3)	0.7462(7)	2.8(1)
N(11)	0.6787(3)	0.1122(2)	0.4645(5)	2.2(1)	C(19′)	0.4515(4)	0.3539(3)	0.5952(6)	2.1(1)
N(12)	0.7432(3)	0.0794(2)	0.4341(5)	2.18(9)	C(20′)	0.4282(3)	0.3017(3)	0.6578(6)	1.8(1)
C(1)	0.7115(3)	0.0082(3)	0.8020(6)	1.9(1)	C(21′)	0.3911(4)	0.2501(3)	0.8125(7)	2.6(1)
C(2)	0.6803(4)	0.0570(3)	0.9015(6)	2.1(1)	C(22′)	0.4098(4)	0.2131(3)	0.6996(6)	2.5(1)
C(3)	0.5480(3)	0.0447(3)	0.8327(6)	1.9(1)	C(23′)	0.4582(5)	0.2268(3)	0.4648(7)	3.3(1)
C(4)	0.5006(3)	0.0556(3)	0.7009(6)	1.7(1)	C(24′)	0.2504(3)	0.4007(3)	1.1824(6)	2.3(1)
C(5)	0.4658(4)	0.0772(3)	0.4889(6)	2.2(1)	C(25′)	0.3063(4)	0.3584(3)	1.2387(7)	2.7(1)
C(6)	0.4112(4)	0.0502(3)	0.5330(7)	2.6(1)	C(26′)	0.3573(4)	0.3500(3)	1.1379(6)	2.5(1)
C(7)	0.3951(4)	0.0042(3)	0.7624(7)	2.8(1)	Cl(1)	0.3982(1)	0.14221(7)	0.1140(2)	2.81(3)
C(8)	0.5795(4)	0.1414(3)	0.9179(6)	2.0(1)	Cl(2)	0.0688(1)	0.36197(8)	0.3837(2)	3.53(4)
C(9)	0.6016(3)	0.1911(3)	0.8493(6)	1.9(1)	Cl(3)	0.61202(9)	0.36309(7)	0.3841(2)	2.63(3)
C(10)	0.6335(4)	0.2417(3)	0.6847(7)	2.5(1)	Cl(4)	0.1565(1)	0.8435(1)	0.1023(3)	5.38(5)
C(11)	0.6230(5)	0.2784(3)	0.7971(8)	3.1(1)	O(11)	0.4588(5)	0.0951(3)	0.1297(8)	6.9(2)
C(12)	0.5875(5)	0.2681(3)	1.0446(8)	3.8(2)	O(12)	0.3514(3)	0.1391(3)	0.2253(7)	5.3(1)
C(13)	0.7948(4)	−0.0109(3)	0.8399(6)	2.1(1)	O(13)	0.4290(4)	0.1963(3)	0.1232(6)	4.9(1)
C(14)	0.8029(4)	−0.0993(3)	0.6816(7)	2.7(1)	O(14)	0.3644(6)	0.1338(4)	−0.0208(8)	7.7(2)
C(15)	0.7923(4)	−0.1091(3)	0.5255(7)	2.4(1)	O(21)	0.0848(4)	0.4210(3)	0.3711(7)	4.5(1)
C(16)	0.7774(4)	−0.0925(3)	0.3053(7)	3.2(1)	O(22)	−0.0005(5)	0.3552(4)	0.304(2)	10.7(3)
C(17)	0.7672(5)	−0.1494(4)	0.3208(8)	3.6(2)	O(23)	0.073(1)	0.3496(5)	0.522(1)	12.9(4)
C(18)	0.7729(6)	−0.2151(4)	0.525(1)	5.0(2)	O(24)	0.1247(4)	0.3229(4)	0.315(1)	6.9(2)
C(19)	0.9130(3)	−0.0482(3)	0.7310(7)	2.4(1)	O(31)	0.6601(3)	0.3843(3)	0.2932(6)	4.8(1)
C(20)	0.9381(3)	0.0047(3)	0.6749(6)	2.0(1)	O(32)	0.6253(4)	0.3806(4)	0.5262(7)	6.1(2)
C(21)	0.9365(4)	0.0787(3)	0.5483(7)	2.8(1)	O(33)	0.6162(9)	0.3034(3)	0.3730(8)	11.7(4)
C(22)	1.0012(4)	0.0748(3)	0.6264(9)	3.4(1)	O(34)	0.5396(4)	0.3860(5)	0.3435(7)	11.5(3)
C(23)	1.0590(4)	0.0076(4)	0.8189(9)	3.9(2)	O(41)	0.1910(5)	0.8684(4)	0.2278(9)	6.9(2)
C(24)	0.6596(4)	0.1495(3)	0.3634(6)	2.6(1)	O(42)	0.1038(7)	0.8912(5)	0.047(1)	11.4(3)
C(25)	0.7121(4)	0.1418(3)	0.2647(7)	2.9(1)	O(43)	0.2131(5)	0.8225(5)	0.0209(9)	9.4(2)
C(26)	0.7641(4)	0.0960(3)	0.3116(6)	2.5(1)	O(44)	0.1178(4)	0.7970(3)	0.1324(9)	7.4(2)
Cu(1′)	0.21115(4)	0.46627(3)	0.91370(7)	1.89(1)	N(13)	0.1038(5)	0.1398(4)	−0.011(1)	6.0(2)
Cu(2′)	0.37979(4)	0.39164(3)	0.85525(7)	1.60(1)	C(27)	0.018(1)	0.2310(7)	0.094(2)	9.7(4)
O(1′)	0.3009(2)	0.4568(2)	0.8125(4)	1.83(7)	C(28)	0.0630(6)	0.1798(5)	0.0388(9)	5.0(2)
N(1′)	0.1612(3)	0.5058(2)	0.7275(5)	2.2(1)	N(14)	0.8299(7)	0.3412(6)	0.578(1)	8.3(3)
N(2′)	0.2010(3)	0.5603(3)	0.9834(6)	2.9(1)	C(29)	0.8131(9)	0.2315(6)	0.518(2)	7.8(3)
N(3′)	0.1834(4)	0.6508(3)	0.9110(7)	3.3(1)	C(30)	0.8232(6)	0.2931(6)	0.556(1)	5.7(2)
N(4′)	0.1099(3)	0.4455(3)	0.9292(6)	2.3(1)	N(15)	0.9691(6)	0.8091(5)	0.554(1)	6.7(2)*
N(5′)	−0.0019(3)	0.4377(3)	0.8196(7)	2.9(1)	C(31)	0.9798(8)	0.7490(6)	0.317(1)	6.6(3)*
N(6′)	0.4098(3)	0.4079(2)	0.6577(5)	1.83(9)	C(32)	0.9734(6)	0.7820(5)	0.452(1)	5.1(2)*
N(7′)	0.4865(3)	0.4198(2)	0.9085(5)	1.88(9)	N(16)	0.879(1)	0.1487(8)	0.986(2)	1.4(3)*
N(8′)	0.5723(3)	0.4664(2)	0.8343(5)	1.96(9)	C(33)	0.924(4)	0.144(3)	1.236(7)	8(1)*
N(9′)	0.4030(3)	0.3058(2)	0.7842(5)	2.15(9)	C(34)	0.898(3)	0.145(2)	1.112(5)	5.4(8)*
N(10′)	0.4326(3)	0.2467(2)	0.6027(5)	2.2(1)	N(17)	0.204(1)	0.318(1)	0.772(2)	6.6(4)*
N(11′)	0.2680(3)	0.4160(2)	1.0574(5)	1.76(9)	C(40)	0.203(1)	0.2698(8)	0.988(2)	3.9(3)*
N(12′)	0.3345(3)	0.3844(2)	1.0300(5)	1.84(9)	C(41)	0.196(1)	0.295(1)	0.865(2)	5.4(4)*
C(1′)	0.2884(4)	0.4703(3)	0.6698(6)	2.3(1)	C(42)	0.224(2)	0.257(2)	1.051(4)	6.0(7)*
C(2′)	0.2062(4)	0.4714(3)	0.6212(6)	2.3(1)	C(43)	0.223(2)	0.328(1)	0.730(3)	4.9(5)*
C(3′)	0.1711(4)	0.5699(3)	0.7270(7)	2.5(1)	C(44)	0.212(1)	0.3039(9)	0.837(2)	2.7(3)*
C(4′)	0.1846(4)	0.5936(3)	0.8736(7)	2.6(1)	C(45)	0.206(1)	0.279(1)	0.935(2)	3.7*
C(5′)	0.2112(4)	0.6000(3)	1.0970(8)	3.4(1)					

[a] Starred values indicate that atoms were refined isotropically. Occupanies: N(15), 0.5; C(31), 0.5; C(32), 0.5; N(16), 0.5; C(33), 0.5; C(34), 0.5; N(17), 0.5; C(40), 0.55; C(41), 0.7; C(42), 0.1; C(43), 0.4; C(44), 0.3; C(45), 0.45.

the complex. In **6A**, Cu(1)−N(11) = 1.963(5) and Cu(2)−N(12) = 1.970(6) Å, while in **6B**, the Cu(1′)−N(11′) and Cu(2′)−N(12′) bond lengths are 1.978(5) and 1.949(5) Å, respectively.

The bond angles around the copper ions in compounds **6A** and **6B** are similar. The Cu(1)−O(1)−Cu(2) bridging angles in **6A** and **6B** are 116.3(2) and 118.9(2)°, respectively, and the angles within the equatorial planes of each complex range from 82 to 102°. In dinuclear cation **6A**, the Cu(1) atom is displaced 0.369(1) Å from the least-squares plane defined by N(1), N(4), N(11), and O(1), while Cu(2) is displaced 0.363(1) Å from the plane defined by N(6), N(9), N(12), and O(1). In dinuclear cation **6B,** the copper ions are displaced 0.350(1) (Cu(1′)) and

(27) (a) Mazurek, W.; Kennedy, B. J.; Murray, K. S.; O'Connor, M. J.; Rogers, J. R.; Snow, M. R.; Wedd, A. G.; Zwack, P. R. *Inorg. Chem.* **1985**, *24*, 3258−3264. (b) Mazurek, W.; Berry, K. J.; Murray, K. S.; O'Connor, M. J.; Snow, M. R.; Wedd, A. G. *Inorg. Chem.* **1982**, *21*, 3071−3080.

Table 3. Positional Parameters with Estimated Standard Deviations and Thermal Parameters for Compound **7**

atom	*x*	*y*	*z*	*B*,[a] Å^2	atom	*x*	*y*	*z*	*B*,[a] Å^2
Cu(1)	0.19985(6)	0.18928(5)	0.96531(7)	2.86(2)	N(10)	0.4245(4)	0.5785(3)	0.8387(6)	3.3(1)
Cu(2)	0.20445(6)	0.41139(5)	0.95392(7)	2.70(2)	N(11)	0.1207(7)	0.9146(6)	0.4297(7)	6.6(2)
Cl(1)	0.4706(1)	0.2456(2)	0.5620(2)	4.45(4)	C(1)	0.2219(5)	0.2500(4)	0.7417(6)	2.6(1)
Cl(2)	0.1417(2)	0.7112(1)	0.7040(2)	4.37(4)	C(2)	0.1787(5)	0.1419(4)	0.6898(6)	2.6(1)
O(1)	0.2462(3)	0.2850(3)	0.8849(4)	2.41(8)	C(3)	0.1474(5)	0.0040(4)	0.7697(6)	2.9(1)
O(2)	0.1942(4)	0.2697(3)	1.1339(4)	3.8(1)	C(4)	0.0448(5)	0.0192(4)	0.8178(6)	2.7(1)
O(3)	0.2496(4)	0.4215(3)	1.1432(4)	3.8(1)	C(5)	−0.0577(5)	0.0869(5)	0.9368(7)	3.4(1)
O(11)	0.5133(5)	0.2218(4)	0.6793(5)	5.1(1)	C(6)	−0.1224(6)	0.0011(5)	0.8564(7)	3.7(2)
O(12)	0.3612(5)	0.1875(7)	0.4899(7)	8.9(2)	C(7)	−0.0909(6)	−0.1359(5)	0.6839(8)	3.9(2)
O(13)	0.5458(4)	0.2340(6)	0.4779(5)	6.8(2)	C(8)	0.3416(5)	0.0978(4)	0.8111(6)	3.1(1)
O(14)	0.4630(6)	0.3432(5)	0.6022(8)	8.2(2)	C(9)	0.3966(5)	0.1164(4)	0.9564(6)	3.1(1)
O(21AB)	0.033(1)	0.6556(8)	0.636(1)	8.9(3)*	C(10)	0.4219(6)	0.1553(5)	1.1713(7)	3.7(2)
O(22AC)	0.1476(9)	0.7882(7)	0.817(1)	7.3(2)*	C(11)	0.5240(6)	0.1462(5)	1.1500(8)	4.4(2)
O(22B)	0.167(3)	0.641(2)	0.596(3)	9.6(8)*	C(12)	0.5953(6)	0.1117(6)	0.9407(9)	4.9(2)
O(22C)	0.218(2)	0.658(1)	0.662(2)	5.6(4)*	C(13)	0.1306(5)	0.2950(4)	0.6793(6)	2.8(1)
O(23A)	0.221(1)	0.666(1)	0.752(2)	6.1(3)*	C(14)	0.0475(6)	0.4321(4)	0.7252(7)	3.6(2)
O(23B)	0.208(1)	0.679(1)	0.825(2)	4.5(4)*	C(15)	−0.0171(5)	0.4004(4)	0.8152(7)	3.3(1)
O(23C)	0.025(1)	0.660(1)	0.696(2)	4.3(3)*	C(16)	−0.0456(6)	0.3578(5)	0.9855(8)	4.4(2)
O(24A)	0.189(1)	0.775(1)	0.637(2)	7.0(4)*	C(17)	−0.1475(6)	0.3499(5)	0.8996(9)	5.0(2)
O(24B)	0.181(2)	0.803(2)	0.722(2)	7.1(5)*	C(18)	−0.2170(7)	0.3748(7)	0.676(1)	6.8(3)
O(24C)	0.120(2)	0.754(1)	0.590(2)	5.9(5)*	C(19)	0.2469(6)	0.4519(4)	0.7095(6)	3.1(1)
N(1)	0.2194(4)	0.1001(3)	0.7941(5)	2.5(1)	C(20)	0.3319(5)	0.5163(4)	0.8344(6)	2.7(1)
N(2)	0.0482(4)	0.0973(3)	0.9118(5)	2.7(1)	C(21)	0.4220(6)	0.5828(4)	1.0447(7)	3.4(2)
N(3)	−0.0560(4)	−0.0418(3)	0.7819(5)	3.0(1)	C(22)	0.4808(5)	0.6213(4)	0.9724(7)	3.5(2)
N(4)	0.3415(4)	0.1361(4)	1.0499(5)	3.0(1)	C(23)	0.4575(6)	0.5945(5)	0.7227(8)	4.7(2)
N(5)	0.5082(4)	0.1219(4)	1.0126(6)	3.5(1)	C(24)	0.2315(5)	0.3569(5)	1.1962(6)	3.3(1)
N(6)	0.1557(4)	0.3982(3)	0.7500(5)	2.5(1)	C(25)	0.2519(7)	0.3864(5)	1.3477(7)	4.4(2)
N(7)	0.0368(4)	0.3899(4)	0.9286(6)	3.3(1)	C(26)	0.324(1)	0.933(1)	0.404(2)	13.2(6)
N(8)	−0.1309(5)	0.3761(4)	0.7941(7)	4.2(2)	C(27)	0.2067(8)	0.9155(6)	0.4212(9)	5.9(2)
N(9)	0.3276(4)	0.5157(3)	0.9548(5)	2.5(1)					

[a] Starred values indicate that atoms were refined isotropically. Occupanies: O(21AB), 0.7; O(22AC), 0.7; O(22B), 0.4; O(22C), 0.4; O(23A), 0.3; O(23B), 0.3; O(23C), 0.3; O(24A), 0.3; O(24B), 0.3; O(24B), 0.3; O(24C), 0.3.

Scheme 1

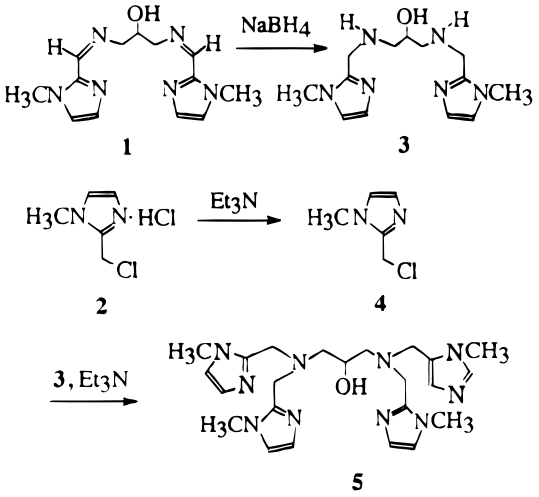

0.420(1) Å (Cu(2′)). Overall, the structures of **6A** and **6B** resemble those of other pyrazolate-bridged complexes,[27−29] and the Cu−O and Cu−N distances are consistent with distances reported for other dinuclear copper(II) complexes containing polyimidazole and benzimidazole ligands.[29−33]

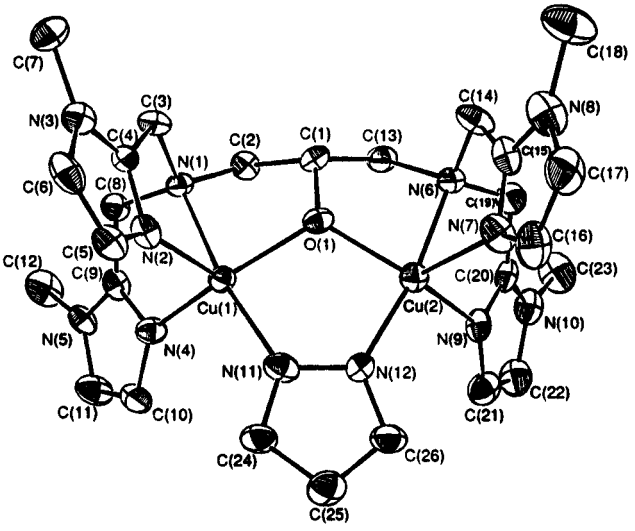

Figure 1. ORTEP view (50% probability ellipsoids) of compound **6A** with labeling scheme.

(b) $[Cu_2(htmihpn)(O_2CCH_3)](ClO_4)_2\cdot CH_3CN$ (7). An ORTEP view of the cation portion of compound **7** is shown in Figure 2. Selected bond distances and angles are given in Table 6. The coordination environments around the copper ions are slightly different. Cu(1) has a distorted trigonal bipyramidal geometry. The equatorial plane of the molecule is defined by Cu(1), N(2), N(4), and O(1). The corresponding bond angles within the trigonal plane are O(1)−Cu(1)−N(4) = 111.7(2)°, O(1)−Cu(1)−N(2) = 127.8(2)°, and N(2)−Cu(1)−N(4) = 114.2(2)°.

(28) Nishida, Y.; Kida, S. *Inorg. Chem.* **1988**, *27*, 447−452.
(29) Doman, T. N.; Williams, D. E.; Banks, J. F.; Buchanan, R. M.; Chang, H.-R.; Webb, R. J.; Hendrickson, D. N. *Inorg. Chem.* **1990**, *29*, 1058−1062.
(30) (a) Sorrell, T. N.; Garrity, M. L. *Inorg. Chem.* **1991**, *30* , 210−215. (b) Sorrel, T. N.; Borovik, A. S. *J. Am. Chem. Soc.* **1987**, *109*, 4255−4260.
(31) Baldwin, M. J.; Root, D. E.; Pate, J. E.; Fujisawa, K.; Kitajima, N.; Solomon, E. I. *J. Am. Chem. Soc.* **1992**, *114*, 10421−10431.
(32) Oberhausen, K. J.; Richardson, J. F.; Buchanan, R. M.; McCusker, J. K.; Hendrickson, D. N.; Latour, J.-M. *Inorg. Chem.* **1991**, *30*, 1357−1365.
(33) (a) Nakao, Y.; Onoda, M.; Sakurai, T.; Nakahara, A.; Kinoshita, I.; Ooi, S. *Inorg. Chim. Acta* **1989**, *165* , 111−114. (b) Nakao, Y.; Onoda, M.; Sakurai, T.; Nakahara, A.; Kinoshita, I.; Ooi, S. *Inorg. Chim. Acta* **1988**, *151* , 55−59.

Table 4. Selected Bond Distances (Å) for Compound **6**

6A		6B	
Cu(1)−Cu(2)	3.320(1)	Cu(1′)−Cu(2′)	3.3462(9)
Cu(1)−O(1)	1.955(4)	Cu(1′)−O(1′)	1.936(5)
Cu(1)−N(1)	2.100(5)	Cu(1′)−N(1′)	2.129(6)
Cu(1)−N(2)	2.176(5)	Cu(1′)−N(2′)	2.207(6)
Cu(1)−N(4)	2.007(5)	Cu(1′)−N(4′)	1.978(6)
Cu(1)−N(11)	1.963(5)	Cu(1′)−N(11′)	1.978(5)
Cu(2)−O(1)	1.953(4)	Cu(2′)−O(1′)	1.950(4)
Cu(2)−N(6)	2.101(6)	Cu(2′)−N(6′)	2.082(5)
Cu(2)−N(7)	2.197(6)	Cu(2′)−N(7′)	2.139(6)
Cu(2)−N(9)	2.005(5)	Cu(2′)−N(9′)	2.042(5)
Cu(2)−N(12)	1.970(6)	Cu(2′)−N(12′)	1.949(5)

Table 5. Selected Bond Angles (deg) for Compound **6**

6A		6B	
Cu(1)−O(1)−Cu(2)	116.3(2)	Cu(1′)−O(1′)−Cu(2′)	118.9(2)
N(1)−Cu(1)−O(1)	82.1(2)	N(1′)−Cu(1′)−O(1′)	83.0(2)
N(1)−Cu(1)−N(2)	79.5(2)	N(1′)−Cu(1′)−N(2′)	79.8(3)
N(1)−Cu(1)−N(4)	83.7(2)	N(1′)−Cu(1′)−N(4′)	83.5(2)
N(1)−Cu(1)−N(11)	170.2(2)	N(1′)−Cu(1′)−N(11′)	167.2(2)
N(2)−Cu(1)−O(1)	106.6(2)	N(2′)−Cu(1′)−O(1′)	101.8(3)
N(2)−Cu(1)−N(4)	105.5(3)	N(2′)−Cu(1′)−N(4′)	104.0(2)
N(2)−Cu(1)−N(11)	107.7(3)	N(2′)−Cu(1′)−N(11′)	111.1(3)
N(4)−Cu(1)−O(1)	141.7(2)	N(4′)−Cu(1′)−O(1′)	148.2(2)
N(4)−Cu(1)−N(11)	100.4(2)	N(4′)−Cu(1′)−N(11′)	99.7(2)
O(1)−Cu(1)−N(11)	89.4(2)	O(1′)−Cu(1)′−N(11′)	88.0(2)
N(6)−Cu(2)−N(7)	79.5(2)	N(6′)−Cu(2′)−N(7′)	79.6(2)
N(6)−Cu(2)−N(9)	84.3(2)	N(6′)−Cu(2′)−N(9′)	82.7(2)
N(6)−Cu(2)−N(12)	170.6(3)	N(6′)−Cu(2′)−N(12′)	169.8(2)
N(6)−Cu(2)−O(1)	82.0(2)	N(6′)−Cu(2′)−O(1′)	81.7(2)
N(7)−Cu(2)−N(9)	105.8(2)	N(7′)−Cu(2′)−N(9′)	105.3(2)
N(7)−Cu(2)−N(12)	106.2(3)	N(7′)−Cu(2′)−N(12′)	107.2(2)
N(7)−Cu(2)−O(1)	107.4(3)	N(7′)−Cu(2′)−O(1′)	112.9(2)
N(9)−Cu(2)−O(1)	140.9(2)	N(9′)−Cu(2′)−O(1′)	135.0(2)
N(9)−Cu(2)−N(12)	101.0(2)	N(9′)−Cu(2′)−N(12′)	102.3(2)
O(1)−Cu(2)−N(12)	89.1(2)	O(1′)−Cu(2′)−N(12′)	88.5(2)

The stereochemistry around Cu(2) is more distorted but still resembles a trigonal bipyramid. The atoms defining the equatorial plane around Cu(2) are O(1), N(7), and N(9), and the corresponding metal−ligand bond angles are O(1)−Cu(2)−N(7) = 109.8(2)°, O(1)−Cu(2)−N(9) = 108.5(2)°, and N(7)−Cu(2)−N(9) = 136.0(2)°. The Cu−Cu separation and Cu(1)−O(1)−Cu(2) bridging angle are 3.359(1) Å and 115.4(2)°, respectively. Interestingly, the Cu−Cu separation in the structurally related $[Cu_2(L-Et)(OAc)]^{2+}$ cation is 3.459(2) Å and the Cu−O−Cu bridging angle is 130.6(5)°.[21] The larger values for metal−metal separation and Cu−O−Cu bridging angle in $[Cu_2(L\text{-}Et)(OAc)]^{2+}$ are likely due to the greater steric bulk exerted between benzimidazole ligands.

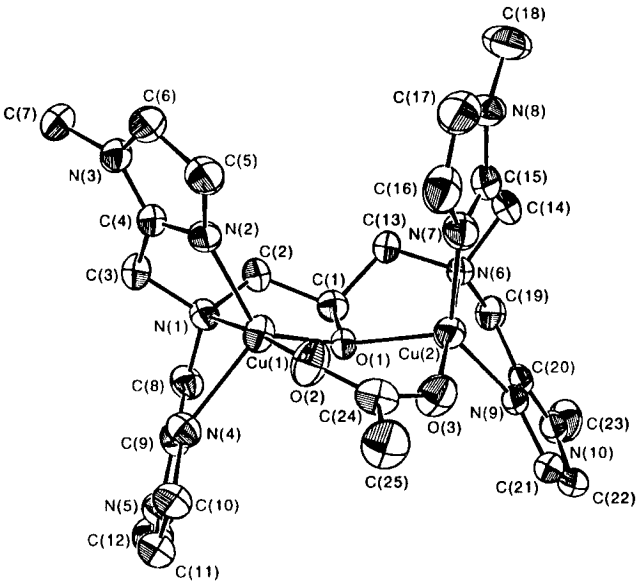

Figure 2. ORTEP view (50% probability ellipsoids) of compound **7** with labeling scheme.

Table 6. Selected Bond Distances (Å) and Angles (deg) for Compound **7**

Bond Distances			
Cu(1)−O(1)	1.927(4)	Cu(2)−O(1)	2.047(4)
Cu(1)−N(1)	2.064(5)	Cu(2)−N(6)	2.081(5)
Cu(1)−N(2)	2.012(4)	Cu(2)−N(7)	1.999(5)
Cu(1)−N(4)	2.164(6)	Cu(2)−N(9)	1.998(5)
Cu(1)−O(2)	1.921(5)	Cu(2)−O(3)	1.939(5)
Cu(1)−Cu(2)	3.359(1)		
Bond Angles			
Cu(1)−O(1)−Cu(2)	115.4(2)		
O(1)−Cu(1)−O(2)	99.2(2)	O(1)−Cu(2)−O(3)	96.7(2)
O(1)−Cu(1)−N(1)	82.6(2)	O(1)−Cu(2)−N(6)	82.4(2)
O(1)−Cu(1)−N(2)	127.8(2)	O(1)−Cu(2)−N(7)	109.8(2)
O(1)−Cu(1)−N(4)	111.7(2)	O(1)−Cu(2)−N(9)	108.5(2)
O(2)−Cu(1)−N(1)	174.6(2)	O(3)−Cu(2)−N(6)	179.1(2)
O(2)−Cu(1)−N(2)	99.9(2)	O(3)−Cu(2)−N(7)	98.2(2)
O(2)−Cu(1)−N(4)	95.6(2)	O(3)−Cu(2)−N(9)	98.2(2)
N(1)−Cu(1)−N(2)	82.9(2)	N(6)−Cu(2)−N(7)	81.8(2)
N(1)−Cu(1)−N(4)	79.0(2)	N(6)−Cu(2)−N(9)	82.4(2)
N(2)−Cu(1)−N(4)	114.2(2)	N(7)−Cu(2)−N(9)	136.0(2)

The Cu(1)−O(1) and Cu(2)−O(1) bond distances in compound **7** are 1.927(4) and 2.047(4) Å, respectively, and are significantly different from those reported for $[Cu_2(L\text{-}Et)(NO_2)]^{2+}$ (1.89(1) and 1.92(1) Å). The Cu−N(amine) bond lengths are 2.064(5) (Cu(1)−N(1)) and 2.081(5) Å (Cu(2)−N(6)), and the Cu−N(imidazole) bond lengths are Cu(1)−N(2) = 2.012(4), Cu(1)−N(4) = 2.164(6), Cu(2)−N(7) = 1.999(5), and Cu(2)−N(9) = 1.998(5) Å. Finally, the acetate ion bridges the two copper ions occupying the apical sites with Cu(1)−O(2) and Cu(2)−O(3) distances of 1.921(3) and 1.939(5) Å, respectively.

Magnetochemistry of Compounds 6 and 7. Variable-temperature dc magnetic susceptibility data were collected on desolvated samples of $[Cu_2(htmihpn)(prz)](ClO_4)_2$ (**6**) and $[Cu_2(htmihpn)(OAc)](ClO_4)_2$ (**7**) in a 10 kG field. For compound **6**, a plot of effective magnetic moment per molecule in the temperature range 4.5−320 K is shown in Figure 3. A moderately strong antiferromagnetic exchange interaction be-

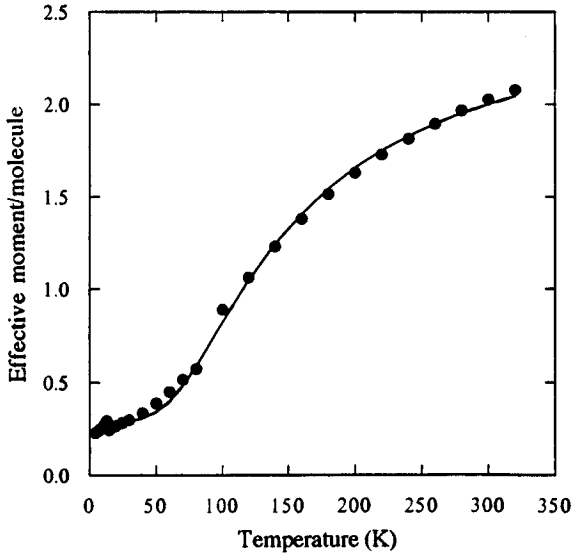

Figure 3. Plot of the effective magnetic moment per dinuclear complex vs temperature for compound **6** between 4.0 and 300 K. The solid line results from a least-squares fit of the data employing a matrix diagonalization approach.

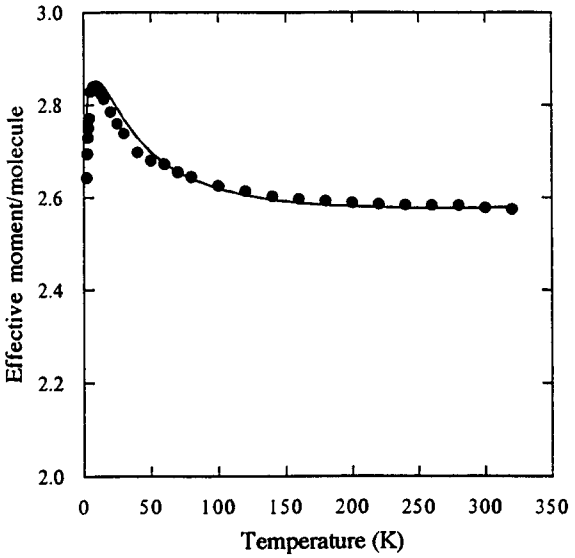

Figure 4. Plot of the effective magnetic moment per dinuclear complex vs temperature for compound **7** between 4.0 and 300 K. The solid line results from a least-squares fit of the data employing a matrix diagonalization approach.

tween Cu^{II} centers is evident. The effective magnetic moment (μ_{eff}) per Cu^{II}_2 decreases gradually from 2.08 μ_B at 320 K to 1.73 μ_B at 220 K and then more rapidly to 0.39 μ_B at 50 K. Below 50 K, μ_{eff} decreases very gradually to 0.23 μ_B at 4.5 K.

The data were analyzed using a single magnetic exchange interaction parameter even though there are slight differences between the coordination environments in the two crystallographically unique dinuclear cations **6A** and **6B**. The 10 kG data were least-squares fit to the Hamiltonian in eq 1.

$$\hat{H} = -2J\hat{S}_1 \cdot \hat{S}_2 + g\mu_B \hat{H}_Z \hat{S}_Z \qquad (1)$$

The first term in eq 1 represents the isotropic Heisenberg exchange interaction and the second term is for an isotropic Zeeman interaction. The Hamiltonian matrix was constructed with a set of uncoupled product base functions using the computer program DIMER.[34] The eigenvalues and eigenvectors were evaluated on each least-squares cycle by diagonalizing the 4×4 Hamiltonian matrix. The paramagnetic susceptibility (χ) of the dimer was then obtained from the calculated magnetization using eq 2, where the derivatives of energy of each level

$$M = \chi H = N\sum[(-\partial E_i/\partial H)\exp(-E_i/kT)]/\sum\exp(-E_i/kT) \qquad (2)$$

with respect to magnetic field ($\partial E_i/\partial H$) were calculated by evaluating slopes. Least-squares fitting was used to fit the temperature dependence of magnetic moments as a function of temperature. The parameters of J (magnetic exchange interaction) and an isotropic g value were evaluated. For compound **6**, a fit for the data was found with $J = -130$ cm^{-1} and $g = 2.0$. The temperature-independent paramagnetism (TIP) was fixed at 120×10^{-6} cgsu, and a paramagnetic of 0.61% weight of monomeric Cu^{II} was included in order to account for the lowest temperature data.

In contrast to compound **6**, two Cu^{II} ions in compound **7** are coupled by a weak ferromagnetic exchange interaction as evident in the plot of μ_{eff}/Cu^{II}_2 vs T (Figure 4). The effective magnetic moment per Cu^{II}_2 increases very gradually from 2.57 μ_B at 320 K to 2.64 μ_B at 80 K, below which the μ_{eff}/Cu^{II}_2 increases more rapidly to 2.84 μ_B at 7 K. Below 7 K, the effective magnetic moment drops sharply to 2.64 μ_B at 2 K. These 10 kG data were least-squares-fit as described above. A good fit of the data occurred with $J = 16.4$ cm^{-1}, $g = 2.02$, TIP $= 120 \times 10^{-6}$ cgsu, and no paramagnetic impurity.

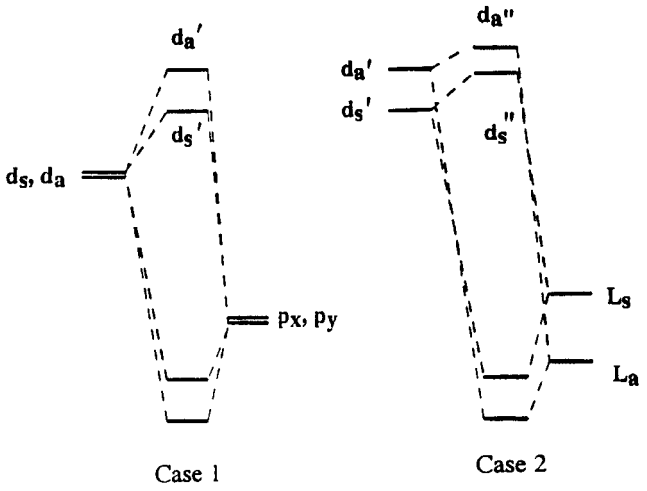

Figure 5. Orbital energy diagrams illustrating the interactions between ligands and metal magnetic orbitals: case 1, for single alkoxo bridge; case 2, for additional bridging ligand. d_s = symmetric magnetic orbitals on Cu(1) and Cu(2) (symmetric with respect to plane perpendicular to N−N bond), d_a = antisymmetric combination, d_a' and d_a'' are antisymmetric combinations and d_s' and d_s'' are symmetric combinations, p_x and p_y = orbitals of bridging oxygen, and L_s and L_a = symmetric and antisymmetric orbitals of bridging ligand, respectively.

Correlation of Structural and Magnetic Data. The different magnetic properties of the pyrazolate- and acetate-bridged complexes may be rationalized as resulting from differences in the coordination geometries around the Cu^{II} ions as well as different metal−ligand magnetic orbital interactions associated with both complexes. Using the *active electron approximation* model, only the magnetic orbitals of the metal and the HOMO's of the bridging ligands were used to rationalize the origin of the magnetic exchange interaction.[1d] In the absence of a second bridging ligand (acetate or pyrazolate), μ-alkoxo-bridged dinuclear copper complexes are antiferromagnetically coupled ($J = -316$ cm^{-1}).[35] The moderately large Cu−O−Cu angles result in good overlap between the copper $d_{x^2-y^2}$ and alkoxo p_x and p_y orbitals. Figure 5 illustrates the energy level diagrams used in rationalizing the magnetic characteristics of both the singly and doubly bridged dinuclear copper complexes.[28] The energy difference between the antisymmetric (d_a') and symmetric (d_s') MO's (case 1) is indicative of the strength of the exchange interaction in μ-alkoxo bridged complexes. In the presence of a second bridging ligand (case 2), either a complementary or noncomplementary effect on the spin exchange interaction may arise due to the further interaction of the ligand symmetric (L_S) and antisymmetric (L_A) combinations with the d_a' and d_s' MO's. This interaction results in the formation of d_a'' (antisymmetric) and d_s'' (symmetric), and the magnitude of the magnetic exchange parameter, J, may be determined according to Hoffmann's expression[16]

$$-2J = \{[E(d_a'') - E(d_s'')]^2 - 2K_{12}\}/(J_{11} - J_{12})$$

where J is the magnetic exchange interaction and K_{12}, J_{11}, and J_{12} are interelectronic repulsion integrals of magnetic orbitals localized on Cu(1) and Cu(2). The interaction of the metal−ligand orbitals thus affects the d_a''−d_s'' energy and determine

(34) Schmitt, E. A.; Hendrickson, D. N. Unpublished results.

(35) Coughlin, P. K.; Lippard, S. J. *J. Am. Chem. Soc.* **1981**, *103*, 3228.

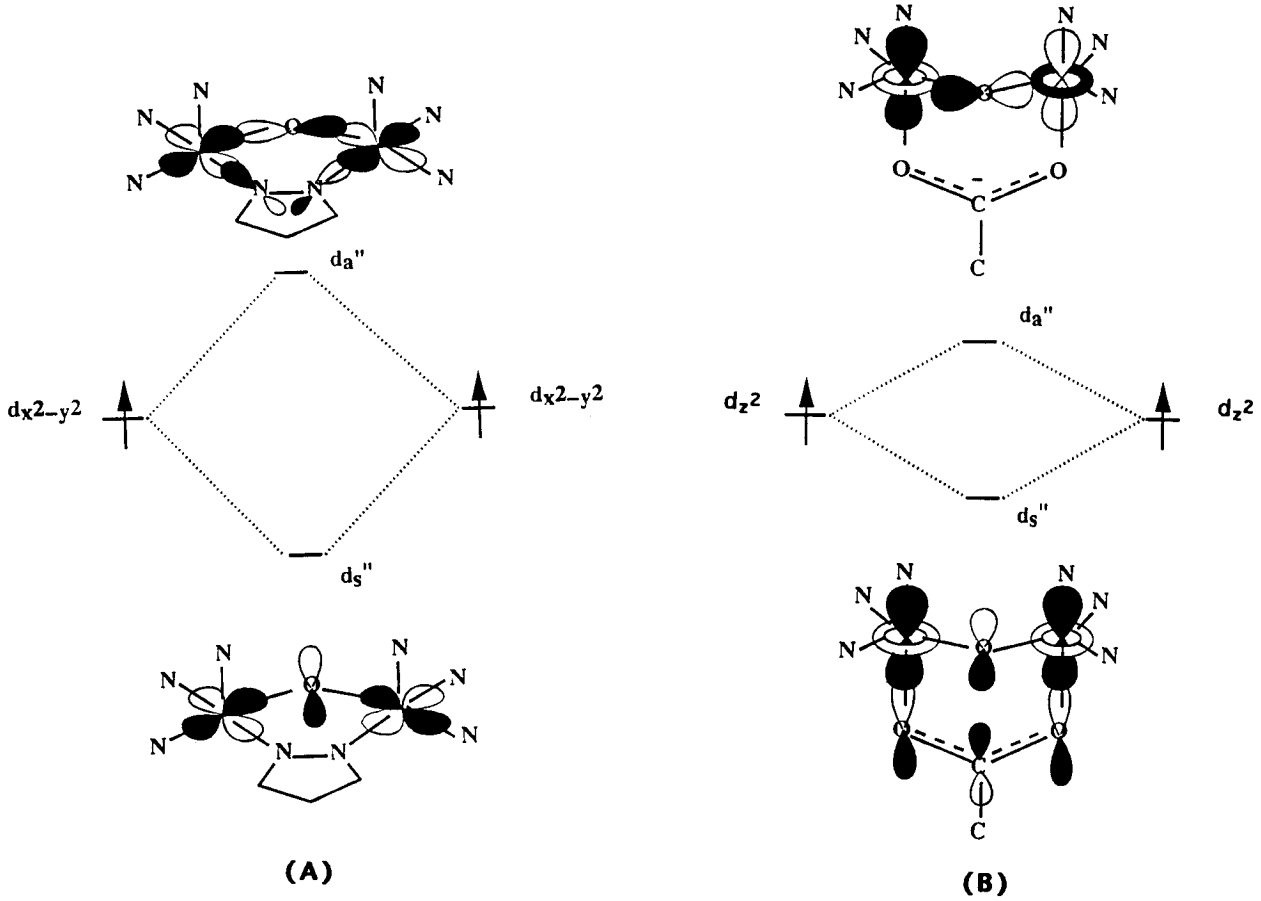

Figure 6. Metal−ligand orbital symmetry combinations: (A) pyrazolate bridge; (B) acetate bridge. d_a is the antisymmetric combination, and d_s is the symmetric combination.

whether the magnetic exchange process results in overall antiferromagnetism or ferromagnetism.

In analyzing the magnetic properties of compounds **6** and **7**, we have utilized the MO diagrams shown in Figure 6 that were generated considering the nearly C_s symmetry observed for the complexes in the solid state. In compound **6**, the distorted square pyramidal geometry of the Cu^{II} ions results in a ground state configuration of the complex dominated by $d_{x^2-y^2}$ orbitals that orient their lobes toward both the alkoxo and pyrazolate bridging ligands. As noted by others,[1a,b] strong antiferromagnetic exchange coupling is anticipated for dinuclear complexes containing $d_{x^2-y^2}$ magnetic orbitals and in compounds where the energy differences between the symmetric (d_s'') and antisymmetric (d_a'') combinations of magnetic orbitals are large.[1a,16] In this case, the $S = 0$ state is lower in energy than the $S = 1$ state, and the singlet−triplet (S−T) splitting is reflected in the magnitude of the exchange parameter J. $[Cu_2(L-Et)N_3]^{2+}$ is an example of a strong antiferromagnetically coupled complex that is essentially diamagnetic at room temperature ($J > -500$ cm^{-1}).[21] The strength of the exchange interaction in this complex has been rationalized in terms of bridging ligand orbital complementarity.[26,28] The azide reinforces the strong coupling mediated by the alkoxide bridge by further destabilizing d_a'' but has no net effect on the energy of d_s''.

The exchange interaction in compound **6** is relatively strong compared to that in other dinuclear Cu^{II} complexes but weaker than the coupling observed for a related series of alkoxide/pyrazolate-bridged complexes, $[Cu_2(L)(prz)]$, where L = 1,3-bis(salicylideneamino)propan-2-ol ($J = -155$ cm^{-1}),[28] 1,4-bis(salicylideneamino)butan-2-ol ($J = -270$ cm^{-1}),[29] and 1,5-bis(salicylideneamino)pentan-3-ol ($J = -297.5$ cm^{-1}),[28] and the related $[Cu_2(L-Et)(NO_2)]^{2+}$ cation ($J = -139$ cm^{-1}).[26] For the $[Cu_2(L)(prz)]$ complexes, Nishida *et al.*[28] and others[29] have argued that the bridging pyrazolate and alkoxo ligand HOMO's tend to stabilize different metal orbital combinations. This leads to a diminution of the separation between d_a'' and d_s'' and a decrease in the antiferromagnetic exchange interaction in these complexes. Similar arguments have been used to rationalize the moderate strength of the exchange coupling observed in $[Cu_2(L-Et)(NO_2)]^{2+}$.[26]

As with the $[Cu_2L(prz)]$ and $[Cu_2(L-Et)(NO_2)]^{2+}$ complexes, ligand orbital complementarity arguments may be used to rationalize the magnitude of the antiferromagnetic exchange in compound **6**. The antisymmetric HOMO of the pyrazolate (Figure 6) combines with the antisymmetric molecular orbital (d_a'), leading to an increase in the $d_a''-d_s''$ and energy separation resulting in stabilization of the singlet ground state. This interaction should favor stronger magnetic exchange coupling through the dominant alkoxide σ spin exchange pathway and result in a stronger antiferromagnetic exchange interaction compared to that in a complex containing only a single alkoxo bridging ligand.[35] Closer inspection of the orbital symmetries of the symmetric combination shows that neither bridging group has a net overlap with the $d_{x^2-y^2}$ orbitals; therefore, no net change in energy of d_s'' is expected with this orbital combination. Clearly, the energy separation between d_a'' and d_s'' is smaller in compound **6** than in the above compounds and the complementary effect on the antiferromagnetic exchange interaction in compound **6** is smaller.

Direct comparison of the structure of compound **6** with those reported for the series of $[Cu_2(L)(prz)]$ complexes and the $[Cu_2(L-Et)(NO_2)]^{2+}$ cation is difficult because the copper ions in compound **6** are five-coordinate, whereas the copper ions in $[Cu_2(L)(prz)]^{2+}$ are four-coordinate, and the $[Cu_2(L\text{-}Et)NO_2]^{2+}$

complex contains a bridging NO_2^- group instead of a pyrazolate ion. Nevertheless, there are significant differences in the structural parameters associated with the bridging alkoxo ligands in these systems that may contribute to the differences in the magnitude of J for the complexes. In both of the dinuclear cations **6A** and **6B**, the Cu−O−Cu bridging angle is more acute (116.3(2) and 118.9(2)°, respectively) than those reported for the $[Cu_2(L)(prz)]$ (average 121.6°) and $[Cu_2(L-Et)(NO_2)]^{2+}$ (127.1(5)°) complexes. In addition the Cu−O and Cu−N bond lengths are different for each complex. The more obtuse angle should favor stronger magnetic exchange coupling due to better overlap between the alkoxide 2p and metal $d_{x^2-y^2}$ orbitals. In addition, Nishida[28] has noted that the $|J|$ values for the $[Cu_2(L)(prz)]$ series of complexes decrease as the chelate ring size decreases from six- to five-membered rings; this is due to an increase in the overlap integral energy associated with the symmetric combination. A similar destabilization of the symmetric combination in compound **6** should result in a decrease in spin coupling relative to a single-alkoxide-bridged system. Thus, it would appear that the strength of the antiferromagnetic exchange interaction in these complexes is dependent not only upon the interaction of ligand HOMO levels with symmetric (d_s'') and antisymmetric (d_a'') combinations of copper magnetic ground state orbitals but also on the arrangement and nature of the ancillary ligands within the coordination spheres and, to a lesser extent, the Cu−O−Cu bridging angles.

In compound **7**, the Cu(II) ions are ferromagnetically coupled ($J = +16.4$ cm^{-1}). The crystal structure of compound **7** shows that the stereochemistry around the copper centers is best described as distorted trigonal bipyramidal. The atoms O(1), N(2), and N(3) define the trigonal plane around the Cu(1) ion, with the largest deviation from ideal trigonal angles being 8.3°. The trigonal arrangement around Cu(2) is more distorted, and the equatorial plane is defined by O(1), N(7), and N(9). The largest deviation of the trigonal angles at the Cu(2) ion is 16°, associated with the N(7)−Cu(2)−N(9) bond angle.

On the basis of the molecular geometry of the Cu(1) ion in compound **7**, it is easy to assign the magnetic ground state orbital to the d_{z^2} orbital. The dominant magnetic orbital of Cu(2) also appears to be the d_{z^2} orbital. In the structurally related $[Cu_2(L-Et)(OAc)]^{+2}$ complex,[21] the magnetic orbitals have been assigned unambiguously to the d_{z^2} orbital of each copper ions. The largest deviation of the trigonal angle for both copper centers was 6.5° in this L-Et complex. It is anticipated that the distortion in the coordination geometry around Cu(2) in compound **7** will lead to some mixing of the $d_{x^2-y^2}$ orbital associated with the square pyramidal geometry with the d_{z^2} ground state of the trigonal bipyramid. Nevertheless, the ferromagnetic coupling observed for **7** may be rationalized by the same arguments used by Reed *et al.*[21] to explain the sign and magnitude of the magnetic exchange interaction in $[Cu_2(L-Et)(OAc)]^{2+}$. As in $[Cu_2(L-Et)(OAc)]^{2+}$, the d_a'' and d_s'' combinations are close in energy and the $S = 1$ state is lower in energy than the $S = 0$ state. Close inspection of the overlap symmetries for the symmetric and antisymmetric combinations of the acetate-bridged complex shows that the alkoxide 2p and acetate a_1 HOMOs[17] tend to stabilize different combinations of the d_{z^2} orbitals, leading to an increase in d_s'' the energy and decrease in the $d_a''-d_s''$ energy difference relative to the single-alkoxide-bridged system.[35]

It is interesting to note that weak antiferromagnetic coupling is observed for a series of $[Cu_2L(OAc)]$ complexes, where L is a Schiff base ligand resulting from the condensation of 1,3-diaminopropan-2-ol and various β-diketones.[36] Nishida and Kida also have rationalized the weak antiferromagnetic exchange coupling observed for these complexes in terms of the noncomplementary interactions of the bridging alkoxide and acetate HOMO's involving, in this case, $d_{x^2-y^2}$ copper magnetic orbitals. Therefore, the ferromagnetic exchange coupling observed for compound **7** appears to be due to noncomplementary interaction between acetate and alkoxide HOMO's and metal d_{z^2} magnetic orbitals. The differences in the magnitude of the ferromagnetic coupling between compound **7** ($J = +16.4$ cm^{-1}) and $[Cu_2(L-Et)(OAc)]^{2+}$ ($J = +12$ cm^{-1}) may be a result of the greater distortion of the coordination environment around Cu(2) in compound **7** compared to the case for the copper ions in $[Cu_2(L-Et)(OAc)]^{2+}$. Binuclear Cu(II) complexes containing both d_{z^2} and $d_{x^2-y^2}$ magnetic ground states are known that exhibit large ferromagnetic exchange coupling due to the *accidental orthogonality*[35,37−39] of the magnetic orbitals.[1a,b,d,17a,35]

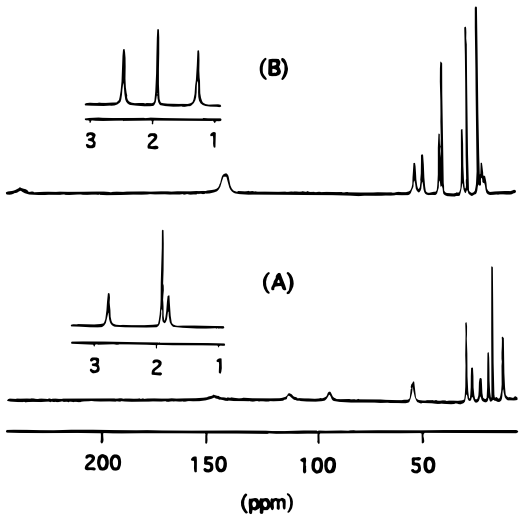

Figure 7. 500 MHz ^{1}H NMR spectra of (A) compound **6** and (B) compound **7** in CD_3CN at 22 °C. The insert portions of the spectra display the two $N-CH_3$ imidazole protons observed for each complex.

^{1}H NMR Spectra of Compounds 6 and 7. Compounds **6** and **7** display well-resolved ^{1}H NMR spectra (Figure 7) despite the differences in the magnitude and sign of the magnetic exchange interactions. Typically, ^{1}H NMR spectroscopy is not readily used to characterize the solution structure of copper(II) complexes due in part to the slow electronic relaxation associated with the paramagnetic copper(II) ions.[40] However there are several examples of binuclear copper(II) complexes that give well-resolved ^{1}H NMR spectra.[14a,41] These compounds contain at least two bridging ligands (alkoxo, phenoxo, or hydroxo ions) that provide a superexchange pathway between the copper(II)

(36) Nishida, Y.; Kida, S. *J. Chem. Soc., Dalton Trans.* **1986**, 2633−2640.
(37) Berends, H. P.; Stephan, D. W. *Inorg. Chem.* **1987**, *26*, 749.
(38) Chaudhuri, P.; Oder, K.; Wieghardt, K.; Nuber, B.; Weiss, J. *Inorg. Chem.* **1986**, *25*, 2818.
(39) Sorrell, T. N.; O'Connor, C. J.; Anderson, O. P.; Reibenspies, J. H. *J. Am. Chem. Soc.* **1985**, *107*, 4199.
(40) Bertini, I.; Luchinat, C. In *Physical Methods for Chemists*, 2nd ed.; Drago, R. S., Ed.; Harcourt Brace Jovanovich: Orlando, FL, 1992; pp 500−556.
(41) (a) Bertini, I.; Turano, P.; Vila, A. J. *Chem. Rev.* **1993**, *93*, 2833−2932. (b) Holz, R. C.; Brink, J. M. *Inorg. Chem.* **1994**, *33*, 4609−4610. (c) Holz, R. C.; Brink, J. M.; Gobena, F. T.; O'Connor, C. J. *Inorg. Chem.* **1994**, *33*, 6086−6092. (d) Wang, S.; Pang, Z.; Zheng, J.-C.; Wagner, M. J. *Inorg. Chem.* **1993**, *32*, 5975−5980. (e) Lubben, M.; Hage, R.; Meetsma, A.; Byma, K.; Feringa, B. L. *Inorg. Chem.* **1995**, *34*, 2217−2224. (f) Maekawa, M.; Kitagawa, S.; Munakata, M.; Masuda, H. *Inorg. Chem.* **1989**, *28*, 1904−1909. (g) Dei, A.; Gatteschi, D.; Piergentili, E. *Inorg. Chem.* **1979**, *18*, 89−93. (h) Byers, W.; Williams, R. J. P. *J. Chem. Soc., Dalton Trans.* **1972**, 555−560. (i) Zelonka, R. A.; Baird, M. C. *Inorg. Chem.* **1972**, *11*, 134−137.

ions, resulting in moderate antiferromagnetic coupling ($-2J = 156-545$ cm^{-1}).

The ^{1}H NMR spectrum of compound **6** displays 12 well-resolved isotropically shifted signals over a chemical shift range of 1−150 ppm, indicating that the basal and apical imidazole donors do not exchange rapidly on the NMR time scale. The signals at 2.85 and 1.85 ppm are assigned to imidazole N−CH_3 protons on the basis of their integrated areas. The remaining signals associated with compound **6** are observed at 147, 112, 93.7, 54.8, 30.2, 27.6, 23.7, 20.0, 18.0, and 13.3 ppm. The signals at 54.8, 30.2, and 13.3 ppm are tentatively assigned to ligand methylene protons on the basis of their integrated areas.

Curiously, compound **7** displays a similar isotropically shifted ^{1}H NMR spectrum, despite the fact that the copper(II) ions are ferromagnetically exchange coupled in the solid state. However, the proton signals are collectively broader than those observed for compound **6** and are shifted over a larger chemical shift range (1−240 ppm). As with compound **6**, only two imidazole N−CH_3 protons are observed at 2.49 and 1.33 ppm for compound **7**. The signal at 23.8 ppm has been definitively assigned to the acetate methyl protons on the basis of deuterium-labeling studies.

Compared to those for compound **6**, the group of proton signals observed between 20 and 60 ppm in the spectrum of **7** are shifted slightly downfield. Interestingly, a more pronounced shift is observed for the proton signal at 141 ppm in the spectrum of compound **7**. A similar doublet signal is observed at 54.8 ppm in the spectrum of compound **6**.

Finally, additional broad signals are observed between 90 and 150 ppm for compound **6** and at 236 ppm for compound **7**. These protons are clearly very close to the paramagnetic centers, which results in their paramagnetic broadening. Definitive assignments of the ligand proton signals of both compounds will require detailed T_1 and 2D COSY studies, which are in progress.

Summary

A new septadentate polyimidazole ligand has been synthesized and found to stabilize dinuclear copper(II) complexes that display different magnetic exchange properties. Compound **6** contains both pyrazolate and alkoxo bridging ligands, and the copper(II) ions are moderately antiferromagnetic exchange coupled. The strength of the exchange interaction in **6** has been rationalized in terms of orbital complementarity effects involving the HOMO levels of the bridging ligands and the metal $d_{x^2-y^2}$ magnetic orbitals. Compound **7**, on the other hand, contains both bridging acetate and alkoxo ligands and is weakly ferromagnetically exchange coupled. The ferromagnetic exchange coupling in **7** appears to be due to noncomplementary interactions between alkoxo and acetate HOMO's and the copper(II) d_{z^2} magnetic orbitals. Finally, both compounds display well-resolved isotropically shifted ^{1}H NMR spectra. Several of the signals have been assigned to specific ligand protons on the basis of integration data and isotopic labeling studies.

Acknowledgment. This work was supported by National Institutes of Health Grants GM45783 (R.M.B.) and HL 13652 (D.N.H.) and National Science Foundation Grants CHE-9016947 (R.M.B.), CHE-9420322 (D.N.H.), and CHE-9016978 (J.F.R.).

Supporting Information Available: Listings of crystallographic experimental details, anisotropic thermal parameters, bond distances and angles, hydrogen atom positional parameters, torsion angles, least-squares planes, dc magnetic data, and ^{1}H NMR spectral data for compounds **6** and **7** (34 pages). Ordering information is given on any current masthead page.

IC9511985